Corrosion Science, Volume 99, October 2015, Pages 66–75, doi:10.1016/j.corsci.2015.06.019

XPS study of the effects of long-term Ar^+ ion and Ar cluster sputtering on the chemical degradation of hydrozincite and iron oxide

R. Steinberger[a], J. Walter[b], T. Greunz[a], J. Duchoslav[a], M. Arndt[c], S. Molodtsov[b,d], D.C. Meyer[b], D. Stifter[a]

[a] Christian Doppler Laboratory for Microscopic and Spectroscopic Material Characterization, Center for Surface and Nanoanalytics, Johannes Kepler University Linz, Altenberger Straße 69, 4040 Linz, Austria

[b] Institut für Experimentelle Physik, TU Bergakademie Freiberg, Leipziger Straße 23, 09599 Freiberg, Germany

[c] voestalpine Stahl GmbH, voestalpine-Straße 3, 4031 Linz, Austria

[d] European X-Ray Free-Electron Laser Facility (XFEL) GmbH, Notkestraße 85, 22607 Hamburg, Germany

Corresponding author: Roland Steinberger, roland.steinberger@jku.at, +43 732 2468 1469;

E-mail: juliane.walter@physik.tu-freiberg.de, theresia.greunz@jku.at, jiri.duchoslav@jku.at, martin.arndt@voestalpine.com, serguei.molodtsov@xfel.eu, Dirk-Carl.Meyer@physik.tu-freiberg.de, david.stifter@jku.at;

Abstract

Monoatomic ion guns mounted on X-ray photoelectron spectrometers are frequently used for depth profiling to determine the depth distribution of various chemical compounds, or for surface cleaning. Sputtering with single ions may cause severe damage to some materials. Hence, in this study the influence of different sputter parameters on the degradation kinetics was examined. For comparison, the potential of Ar cluster sputtering was tested with the same materials, namely hydrozincite and FeO – two representatives of corrosion products that are susceptible to degradation. Chemical damage could only be minimized by cooling or cluster sputtering within a narrow cluster energy window.

Keywords

A. Zinc; A. Iron; B. Erosion; B. XPS; C. Rust; C. Kinetic parameters;

1. Introduction

In corrosion science, the characterisation of corrosion products is of high importance in order to understand the underlying processes. Depending on the materials investigated, analytical methods with high surface sensitivity that are capable of examining thin layers or interfaces may be required. This brings well-established techniques such as X-ray diffraction close to their limits. Substantial knowledge of surface composition, in terms of chemical compounds, and of the layers directly below, *i.e.*, the depth distribution of compounds or gradients and the transitions at interfaces, is of great interest. X-ray photoelectron spectroscopy (XPS) perfectly meets these requirements, since this method is surface-sensitive and well suited to resolving different chemical states. Tasks such as determining depth distributions are frequently required in the industrial context of various coating systems, for instance, for Zn and Zn-alloy protective layers, passivation and conversion coatings. A simple and cost-effective way of accomplishing these analytical tasks is using a monoatomic ion gun that removes the surface in layers by ion bombardment, as routinely employed in combination with surface sensitive techniques. Recently published studies (*e.g.*, [1,2,3,4]) show that this concept continues to be of high relevance. However, the main drawback is that sputtering may cause sample modification and severe damage (*e.g.*, by preferential sputtering, atomic mixing, or ion implantation, which leads in worst case to chemical changes) to the materials investigated, as already reported for potential corrosion products of Zn and Zn-based coatings [5], nanocomposite coatings [6], and organic materials [7].

Hence, this study examined modifying sputter parameters in order to prevent or reduce the impact of chemical alteration in the context of monoatomic ion sputtering. We considered variations of the etch parameters, in particular acceleration voltage, the gas used and sample temperature (*i.e.*, cooling to low temperatures). As shown in our previous study [5], some Zn-based corrosion products and also iron oxides, which are relevant if corrosion has already advanced substantially, suffer enormous damage. The present work focused on Fe(II) oxide and hydrozincite as two representative corrosion products that are susceptible to degradation. Furthermore, the potential of newer and more sophisticated sputter systems such as cluster guns [8,9] was tested using both materials, since the operation of such devices (*e.g.*, providing Ar clusters and buckminsterfullerene C_{60} clusters) has already shown promising results in other fields [7,10,11,12,13].

2. Materials and methods

2.1. Sample preparation

High purity reference materials of $Zn_5(CO_3)_2(OH)_6$ (hydrozincite) and FeO (iron(II) oxide) from Sigma Aldrich Austria were used in our investigations. Since both materials were available as powders, they were pressed onto pieces of indium foil, filled into polymer blocks with sufficiently large milled circular pockets in the centre, or applied to pieces of adhesive carbon tape.

2.2. Instrumentation

XPS measurements regarding the monoatomic sputter experiments were performed with a Theta Probe system from ThermoFisher (UK) at JKU Linz, and the Ar cluster gun experiments with an Escalab 250Xi system, also from ThermoFisher (UK), at TU Freiberg. Both instruments were controlled by the Avantage software package provided by the system manufacturer, which also enabled data acquisition and evaluation. Each system was equipped with a monochromated Al-K_α X-ray excitation source (1486.7 eV), which was operated at high voltages of 15 kV and 13 kV with emission currents of 3 mA and 4 mA (45 W and 52 W), respectively, and a spot size of 200 µm on the sample. In order to increase the number of photoelectrons moving towards the input lens, the Escalab 250Xi can be operated with a magnetic immersion lens. The electron energy analysers of both spectrometers - hemispherical sector types - were ran in constant analyser energy mode with an energy channel step width of 0.1 eV or 0.05 eV and with the pass energy set to 50 eV, since this is a reasonable compromise between obtainable intensity and energy resolution. In order to compensate for charges building up on the sample surface, the Theta Probe system was equipped with a standard dual flood gun which provides low-energy electrons (typically -2 eV) and simultaneously Ar^+ ions with low kinetic energy. In addition to an external flood gun for low-energy Ar^+ ions, the Escalab 250Xi used an in-lens flood source that provides electrons with low kinetic energy. The sputter experiments performed on the Theta Probe apparatus (base pressure in the low 10^{-9} mbar range, operation pressure in the lower half of the 10^{-7} mbar range) were carried out using a monoatomic Ar^+ ion gun which can be operated with different sets of parameters for acceleration voltage and ion current. Furthermore, using a sputter gun with exchangeable gas supply (mounted on a preparation chamber attached to the XPS system, base pressure 10^{-11} mbar, sputter operation pressure approximately 1 x 10^{-5} mbar) allowed the impact of sputtering with He^+ ions to be tested. The other apparatus - Escalab 250Xi (base pressure in the low 10^{-10} mbar range, operation pressure approximately in the 4×10^{-7} mbar range) -

was equipped with an Ar cluster gun (MAGCIS ion gun from ThermoFisher, UK) which is able to provide both small and large clusters (1000 atoms or 2000 atoms, respectively) with different kinetic energies (2, 4, 6 or 8 keV). Furthermore, the cluster gun can be operated in a monoatomic Ar^+ ion mode. Data analysis of the spectra was based on elimination of the peak backgrounds by applying Shirley background subtraction followed by a peak area normalisation using Scofield sensitivity factors in order to obtain the elemental composition.

2.3. Measurement procedure

High-resolution scans of the photoelectron levels of interest and – when additionally needed – those associated with Auger transitions were acquired in the centre of the sputtered crater, followed by a subsequent sputter step. Duration and number of the sputter steps varied from experiment to experiment; for a detailed description of the sputter sequences see the Results and Discussion section. For monoatomic sputter etching, the angle of incidence was 45°, and a crater size of 2 × 2 mm^2 was chosen, except for He^+ etching, where the corresponding ion gun irradiated a larger area (Gaussian beam profile with a full width at half maximum (FWHM) of 3.5 mm) and raster-scanning the surface with a narrowly focused ion beam was not possible. Operating the ion gun of the Theta Probe XPS with argon gas with 3 keV acceleration voltage, 1 µA ion current and with the above-mentioned crater area (standard parameters as suggested by the manufacturer) allows a sputter rate of ~3.3 nm/min to be achieved on a Si standard. In the Ar cluster gun experiments, where the angle between incident cluster beam and sample surface was 30°, a crater size of only 1 × 1 mm^2 was chosen (i) since no significant influence of edge effects was expected due to the shallow crater depth and (ii) to minimize experimental time. For an estimation of sputter rates of clusters on inorganic compounds it is referred to a study on Ar cluster sputtering of Ta_2O_5 thin films, which revealed for the given setup a removal rate of approximately 0.06 nm/min with a cluster energy of 6 keV [13].

FeO was characterized by means of high-resolution scans of the C1s, O1s, and Fe2p peaks; for hydrozincite the C1s, O1s, Zn2p, and $ZnL_{23}M_{45}M_{45}$ spectra were of interest. Taking the adventitious carbon signal for charge shift correction was not necessary, since the absolute binding energy values were irrelevant to the data evaluation. In most cases, a lack of this carbon species rendered charge shift correction inapplicable. Instead, the modified Auger parameter (MAP) approach [14] – a powerful method for resolving and identifying different chemical states – was applied in the case of hydrozincite to have a practicable marker for the chemical states and to assess long-term stability. In the case of iron oxides, the separation between the photoelectron lines and their corresponding shake-up satellites contains unique information about the oxidation state [15]. Using reference spectra and Gaussian-

Lorentzian-shaped peaks enabled fitting of the data in order to determine the kinetics of the decomposition processes.

3. Results and Discussion

This section describes the impact of monoatomic Ar^+ ion sputtering on hydrozincite and iron(II) oxide when using different sets of etch parameters. The data and results obtained from Ar cluster gun experiments – again tested on hydrozincite and iron(II) oxide – are then presented. In addition, we report the results of first experiments in which hydrozincite was bombarded with He^+ ions.

3.1. Ar^+ ion sputtering on $Zn_5(CO_3)_2(OH)_6$

Based on the results presented in one of our previously published studies in which we investigated the stability of various potential corrosion products (zinc oxide, zinc phosphate, hydrozincite, simonkolleite, Cr(III) oxide, Cr(VI) oxide, Cr(II) chloride, Fe(II) oxide, Fe(III) oxide, and Fe(II, III) oxide) during standard long-term Ar^+ ion sputtering using 3 keV and 1 µA [5], this study focused on variation of the sputter parameters; in particular, we used the following sets including decreased acceleration voltages and/or ion currents: 3 keV and 1 µA, 1 keV and 1 µA, and 1 keV and 0.5 µA. In the experiments, the sputtering periods were: 400 s repeated 25 times, followed by 2000 s repeated 10 times and 4000 s repeated 3 times. The changes of the elemental composition of hydrozincite as a function of the sputter time were found for all parameters to be in accordance to the already reported ones of the recent sputter study with an initial value of the carbonate-to-zinc ratio of ~0.25 and steadily decreasing [5]. Fig. 1 illustrates the evolution of the O1s spectra, which provide the relevant and most pronounced indications for chemical changes, over the etch time both qualitatively and quantitatively for the different sputter parameters.

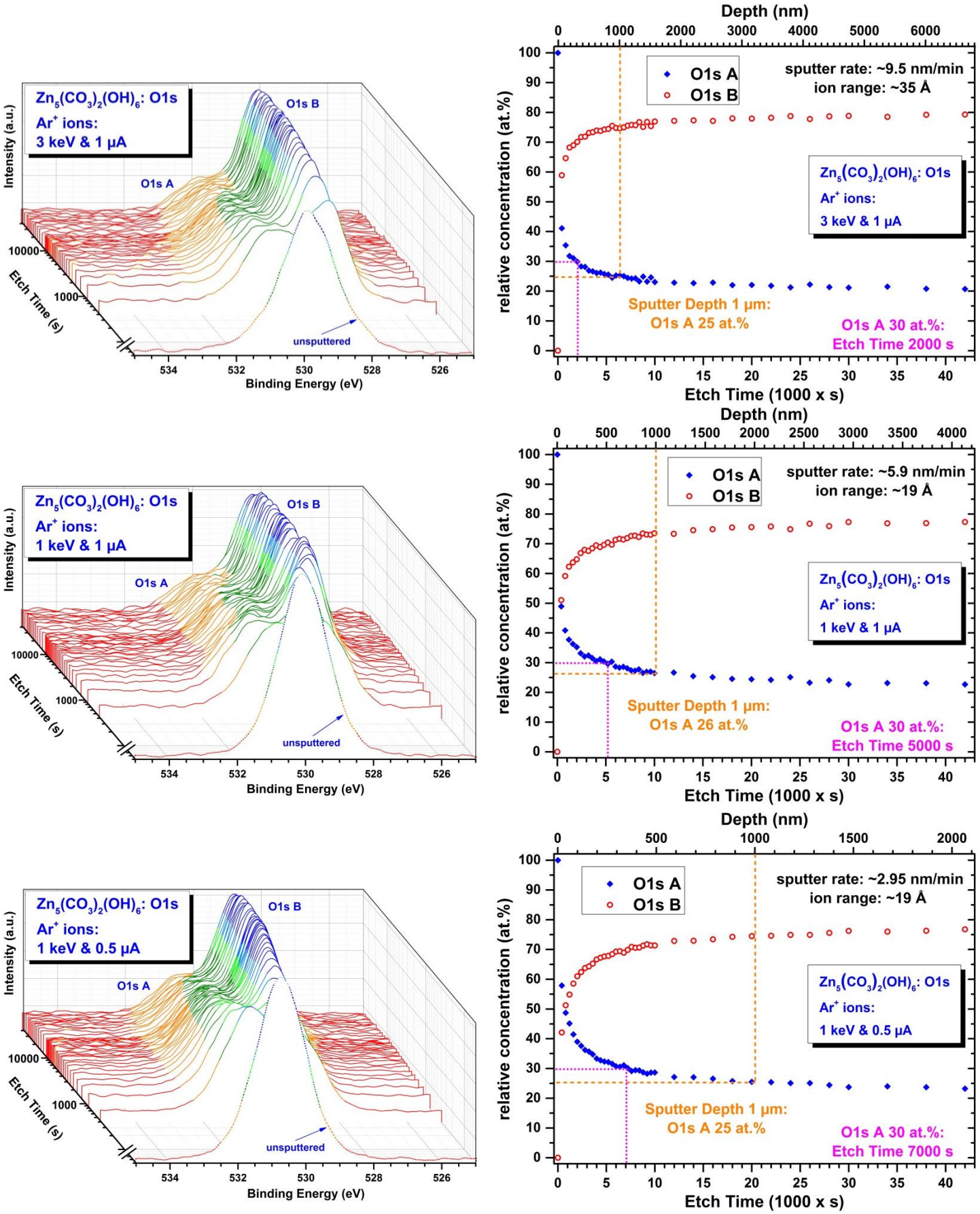
Zn5(CO3)2(OH)6: O1s
Ar+ ions:
3 keV & 1 µA
O1s A
O1s B
Intensity (a.u.)
Etch Time (s)
10000
1000
unsputtered
534
532
530
528
526
Binding Energy (eV)
Depth (nm)
0
1000
2000
3000
4000
5000
6000
O1s A
O1s B
sputter rate: ~9.5 nm/min
ion range: ~35 Å
relative concentration (at.%)
Zn5(CO3)2(OH)6: O1s
Ar+ ions:
3 keV & 1 µA
Sputter Depth 1 µm:
O1s A 25 at.%
O1s A 30 at.%:
Etch Time 2000 s
Etch Time (1000 x s)
Zn5(CO3)2(OH)6: O1s
Ar+ ions:
1 keV & 1 µA
sputter rate: ~5.9 nm/min
ion range: ~19 Å
Sputter Depth 1 µm:
O1s A 26 at.%
O1s A 30 at.%:
Etch Time 5000 s
Zn5(CO3)2(OH)6: O1s
Ar+ ions:
1 keV & 0.5 µA
sputter rate: ~2.95 nm/min
ion range: ~19 Å
Sputter Depth 1 µm:
O1s A 25 at.%
O1s A 30 at.%:
Etch Time 7000 s

Fig. 1 Evolution of the O1s spectra of hydrozincite as functions of sputter time, acquired during long-term Ar^+ ion sputtering using different sets of etch parameters (3 keV and 1 µA, 1 keV and 1 µA, 1 keV and 0.5 µA). The deduced decomposition kinetics of O1s A to O1s B over etch time are additionally shown for each set.

It shall be noted that the corresponding C1s as well as Zn2p levels do not reveal any peculiar change in peak shape and position. However, the O1s spectra clearly show that – independently of the parameters chosen, and even for low kinetic energy and low ion current – chemical damage or alteration of the sample cannot be prevented; the formation of a new kind of oxygen species is evident. In accordance with our previous study (Ar^+ ion bombardment with 3 keV and 1µA) [5], the data again indicate a conversion from hydrozincite to a compound containing mainly zinc oxide. In this context, the sample sputtered by ions with 1 keV and 1 µA exhibited a MAP of 2009.61 ± 0.15 eV and an energy difference between the main peaks of Zn2p and O1s of 491.15 eV; in the case of 1 keV and 0.5 µA, the results were similar (MAP 2009.56 ± 0.12 eV, energy difference 491.13 eV). Also the experiment with 3 keV and 1 µA yielded values in close agreement with the other experiments (MAP 2009.83 ± 0.12 eV, energy difference 491.22 eV). Analysis of the general elemental composition revealed again a rise in the Zn content, while the oxygen content decreased and the carbonate contribution was nearly completely depleted, with a Zn/O ratio as measured for ZnO. Quantitative evaluation of the two O1s peaks, which allows only a comparison of the degradation kinetics, was based on Gaussian-Lorentzian-shaped peaks. Using reference spectra of zinc oxide and hydrozincite for the evaluation may not be advisable, since sputter processes are too complex to clearly identify each product or sub-product formed. The quantitative data (relative concentration plots of O1s A and O1s B in Fig. 1) showed that in the experiment using the highest acceleration voltage the sputter damage (*i.e.*, formation of the new oxygen peak) clearly proceeded faster than in that with lower voltage and identical ion current; for low acceleration voltage and half the ion current, the lowest level of decomposition kinetics was observed. Comparing the etch times at which only 30 at.% of the O1s A type were left yields specific values which support this observation: for 3 keV and 1 µA it was 2000 s, for 1 keV and 1 µA 5000 s and for 1 keV and 0.5 µA 7000 s (cf. the corresponding plots in Fig. 1). After a certain period of time, the oxygen ratios were found to approach similar values, and this trend continued to the end of the measurement, where all 3 curves reached values close to a 20:80 ratio. It is noteworthy that this ratio is in good agreement with the results of fitting the O1s level of a briefly sputter cleaned ZnO reference sample (which exhibits a main peak and a side peak of low intensity at the higher binding energy side) as performed here. The Transport of Ions in Matter (TRIM) software package [16] was used to determine the penetration depth of the argon ions, and based on the sputter yields obtained the sputter rates of model materials (*i.e.*, of materials that contain the same number and

kinds of atoms as hydrozincite and ZnO) were estimated for the exposure to different sets of etch parameters. However, the presented sputter rates should only be taken as approximate values, as they may not accurately reflect the true absolute removal rates, because our simulations cannot take into account chemical bonds of the compounds or changing sputter yields due to a change in sample composition. Nevertheless, relative comparison of the etch rates is much more reliable. Hydrozincite bombarded with 3 keV and 1 µA Ar^+ ions exhibited an ion range of 35 Å and a sputter rate of ~9.5 nm/min; for 1 keV and 1 µA Ar^+ ions, the simulated ion range was 19 Å and the roughly estimated sputter rate ~5.9 nm/min, and for 1 keV and 0.5 µA the predicted sputter rate was ~2.95 nm/min. Further useful information was obtained in these simulations, namely the average surface binding energy; this is an indicator of the energy transfer needed for successful sputter removal of atoms, and amounted to 3.6 eV and 1.7 eV for hydrozincite and zinc oxide, respectively. Using the sputter rates obtained, the quantitative plots in Fig. 1 were complemented with an additional axis for the nominal depth. This axis enables direct comparison of the sputter induced degradation for the different sets of etch parameters relative to the nominally reached sputter depth. Examining, for example, the value of the remaining amount of O1s A type when a depth of 1 µm was reached reveals that the sputter damage is similar (the ratio of O1s A to O1s B is ~25:75) for all sputter conditions used. Furthermore, as expected and indicted by the data, the ion current in the selected experimental range seems to have no significant influence on the alteration of the chemical composition. This is in agreement with Wehner [17], who pointed out that the time between two hit events on the same atom is too long (compared to the frequency of lattice vibrations, which is of the order of 10^{12} to 10^{13} s^{-1}) due to the relatively small ion current densities. Nevertheless, the sputter rate is directly influenced, since the ion current acts as a proportional factor; *i.e.*, theoretically, half of the sputter time is needed to reach the same depth when the ion current is doubled. This implies an extended exposure to ion bombardment when using lower ion currents, which causes very similar damage, as indicated by the quantitative plots in Fig. 1. This is primarily due to the fact that the depth to which the impinging ions cause damage (given by the ion ranges) is greater than the depth from which sample atoms are removed. The escape depth of the hit atoms in the target material is usually below 10 Å [18,19]. Furthermore, the relative O1s A and O1s B data of hydrozincite as a function of sputter depth indicate that, for larger depths, the acceleration voltage does not have such a significant influence on the degradation kinetics as expected. In the case of shallow sputtering, the contribution of the acceleration voltage seems to be greater. In general, the higher the kinetic energy of the ions, the more energy can be transferred to the target and the larger the ion range; *i.e.*, the ratio of damaged to removed volume is far less favourable than when using ions with lower kinetic energy.

As previously shown, a decrease in the kinetic energy of the argon ions is not sufficient to avoid chemical alteration in the material of interest. We also tested another approach: cooling the sample to a low temperature (-135°C) that is maintained during the experiment (for 1 keV and 1 µA). This has already been employed in some other fields of XPS analysis to efficiently prevent or considerably slow down degradation processes [20,21]. The resulting qualitative and quantitative evolution of the O1s levels is shown in Fig. 2.

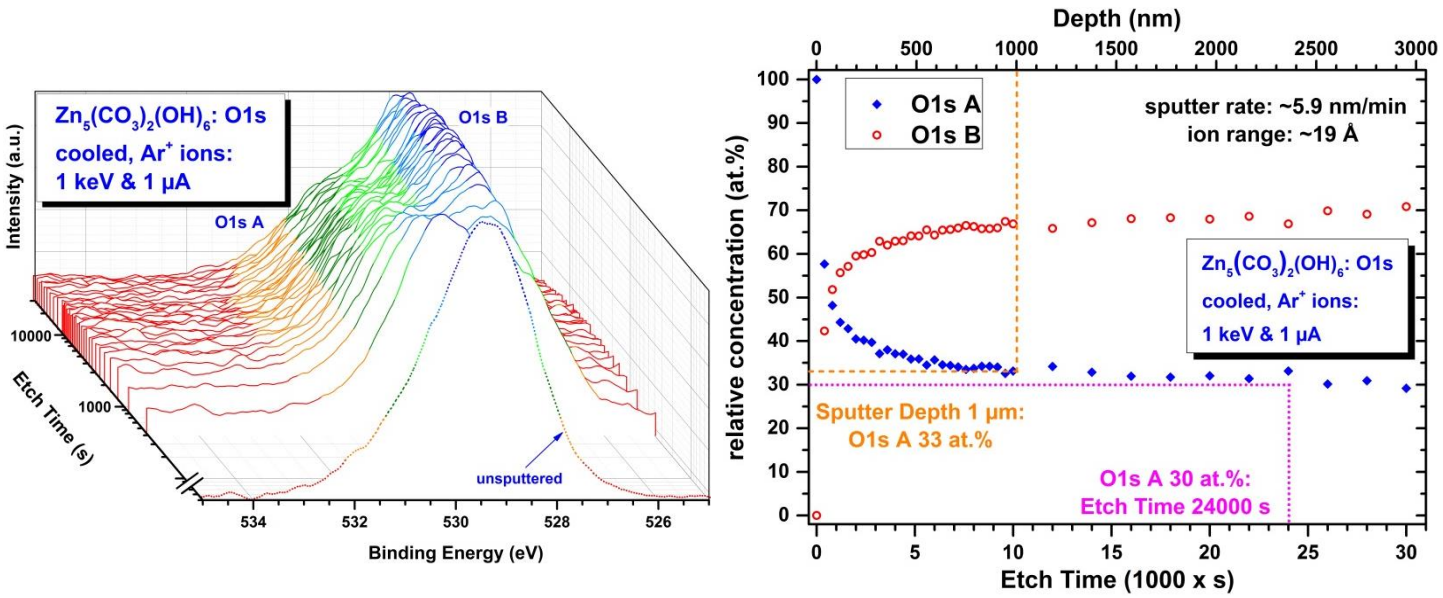

Fig. 2 Evolution of the O1s spectra of hydrozincite, cooled to low temperature (-135 °C), as functions of sputter time, acquired during long-term Ar^+ ion sputtering using an acceleration voltage of 1 keV and an ion current of 1 µA. The deduced decomposition kinetics of O1s A to O1s B over etch time are presented in addition.

However, this approach also could not avoid transformation of the initial chemical compound into another species, as clearly shown by the O1s spectra. Here, the unsputtered surface level suffered a minor distortion of the peak shape towards higher binding energies induced by charging effects, since a perfect charge compensation could not be fully established due to the complexity of the cooling setup. One can see that, compared to the uncooled experiments, the degradation kinetics were the slowest; for instance, it took 24000 s to cause damage such that only 30 at.% of the O1s A type were left. The effect of the target temperature on the sputter yield and thus the sputter rate has been investigated for a large number of different elements and compounds in both polycrystalline and single-crystal form (*e.g.*, [17,22,23,24]). In general, the results indicate that sputter yields may be dependent on – and sometimes independent of – the temperature, as they are determined by a large number of factors, such as chemical composition,

morphology, orientation and sputter parameters. In the case of the cooled hydrozincite sample, assuming the sputter rate to be the same as for the uncooled one exposed to an identical set of parameters, a new axis showing the sputter depth was added to the quantitative plot in Fig. 2. When a nominal sputter depth of 1 μm was reached, the O1s A signal was still at 33 at.%, which indicates that cooling slowed down the damage. Even if the true sputter rate was only one third of that assumed, sample degradation would still be lower than in the uncooled cases.

3.2. Ar^+ ion sputtering on FeO

Recently, we also investigated the influence of Ar^+ ion sputtering on various iron oxides, which might be of importance to various branches of corrosion study [5]. In the present work, we used more "gentle" acceleration voltage and ion current parameters for long-term sputtering: 1 keV and 1 μA, and 1 keV and 0.5 μA. In the experiments, the sputtering periods were: 400 s repeated 25 times, followed by 2000 s repeated 10 times and 4000 s repeated 3 times. In Fig. 3 the quantitative and qualitative evolution of the Fe2p spectra - which provide all valuable information on the chemical oxidation states with evidence included, if metallic iron is present [5] - is shown for different sets of parameters: 3 keV and 1 μA, 1 keV and 1 μA, and 1 keV and 0.5 μA.

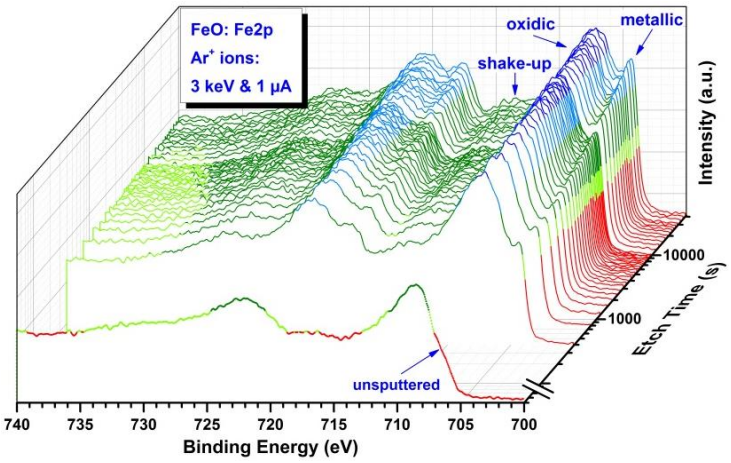
FeO: Fe2p
Ar+ ions:
3 keV & 1 µA
oxidic
metallic
shake-up
unsputtered
Intensity (a.u.)
Etch Time (s)
10000
1000
740 735 730 725 720 715 710 705 700
Binding Energy (eV)

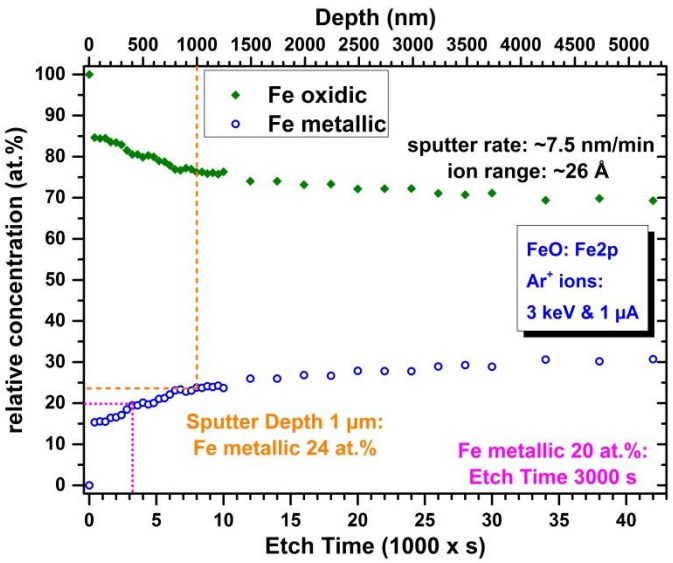
Depth (nm)
0 500 1000 1500 2000 2500 3000 3500 4000 4500 5000
Fe oxidic
Fe metallic
sputter rate: ~7.5 nm/min
ion range: ~26 Å
FeO: Fe2p
Ar+ ions:
3 keV & 1 µA
Sputter Depth 1 µm:
Fe metallic 24 at.%
Fe metallic 20 at.%:
Etch Time 3000 s
relative concentration (at.%)
Etch Time (1000 x s)

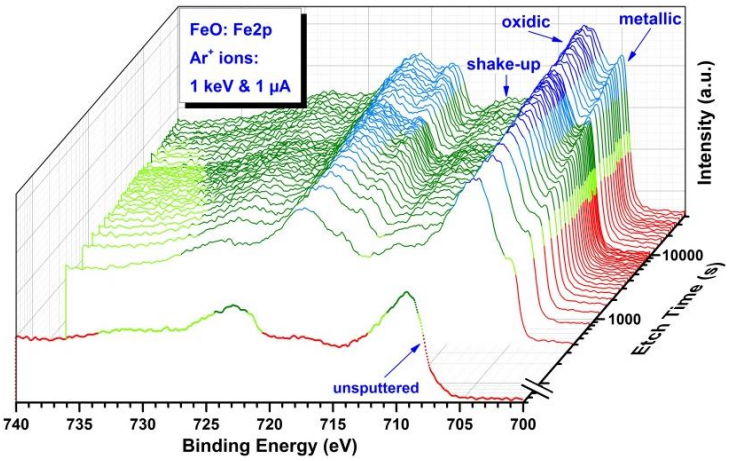
FeO: Fe2p
Ar+ ions:
1 keV & 1 µA
oxidic
metallic
shake-up
unsputtered
Intensity (a.u.)
Etch Time (s)
10000
1000
740 735 730 725 720 715 710 705 700
Binding Energy (eV)

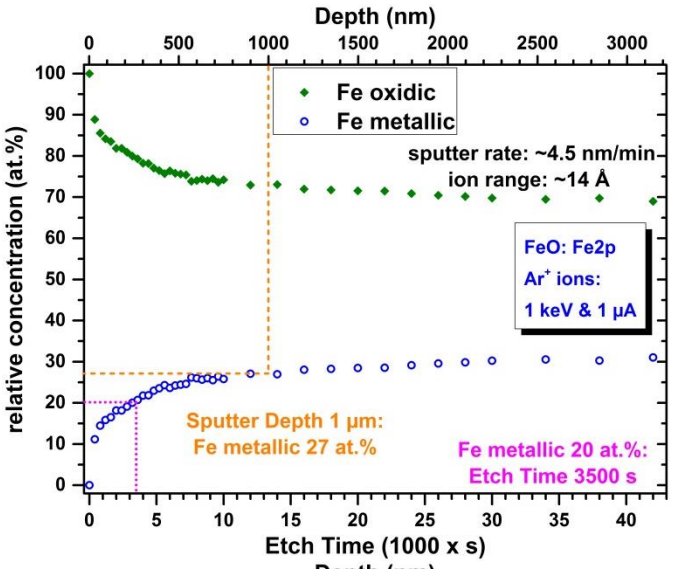
Depth (nm)
0 500 1000 1500 2000 2500 3000
Fe oxidic
Fe metallic
sputter rate: ~4.5 nm/min
ion range: ~14 Å
FeO: Fe2p
Ar+ ions:
1 keV & 1 µA
Sputter Depth 1 µm:
Fe metallic 27 at.%
Fe metallic 20 at.%:
Etch Time 3500 s
relative concentration (at.%)
Etch Time (1000 x s)

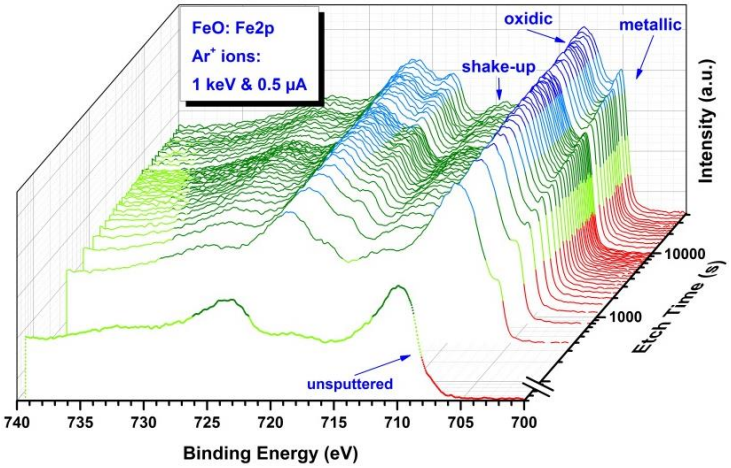
FeO: Fe2p
Ar+ ions:
1 keV & 0.5 µA
oxidic
metallic
shake-up
unsputtered
Intensity (a.u.)
Etch Time (s)
10000
1000
740 735 730 725 720 715 710 705 700
Binding Energy (eV)

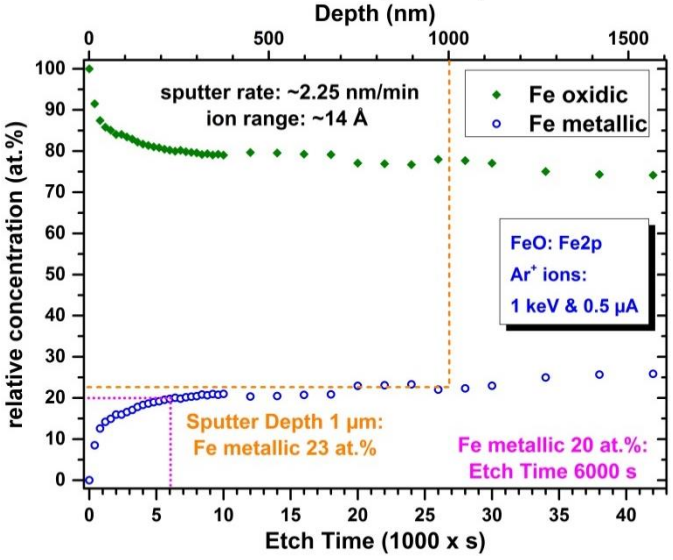
Depth (nm)
0 500 1000 1500
sputter rate: ~2.25 nm/min
ion range: ~14 Å
Fe oxidic
Fe metallic
FeO: Fe2p
Ar+ ions:
1 keV & 0.5 µA
Sputter Depth 1 µm:
Fe metallic 23 at.%
Fe metallic 20 at.%:
Etch Time 6000 s
relative concentration (at.%)
Etch Time (1000 x s)

Fig. 3 Evolution of the Fe2p spectra of iron(II) oxide as functions of sputter time, acquired during long-term Ar^+ ion sputtering using different sets of etch parameters (3 keV and 1 µA, 1 keV and 1 µA, 1 keV and 0.5 µA). The deduced decomposition kinetics of oxidic to metallic type over etch time are additionally shown for each set.

All of the initial iron-to-oxygen ratios were found to be close to 25 to 75 at.%, rapidly increasing to a final value of approximately 45 to 55 at.% after extended sputter time, which is in good agreement to literature studies where the initial and topmost surface composition is attributed to a surface species other than FeO on such powder samples (*e.g.* Fe_2O_3 and hydroxide species) [5,25,26]. It can clearly be seen that none of the sputter configurations chosen could successfully prevent a reduction process to lower oxidation states. The Fe2p spectra suggest a transformation from the oxidic iron species to a metallic one. These qualitative data already indicated that the sputter damage proceeds faster for the 3 keV and 1 µA conditions than for 1 keV and 1 µA, with the slowest kinetics obtained in the experiment with 1 keV and 0.5 µA. Closer inspection of the first etch levels indicated that the reason for the shifting of the shake-up satellites visible in all the plots is that the Fe(II) species is initially covered by a thin Fe(III) layer, as reported in [25,5]. An examination of the separation of the photoelectron peaks and corresponding shake-up satellites gave ~7.9 eV for the surface levels and ~6.2 eV for the following levels. These separations remained approximately constant throughout the experiments, which is in good agreement with the results of Chuang *et al.* [26] and Steinberger *et al.* [5]. To provide a rough overview of the transformation from oxidic to a metallic state (shown in the relative concentration plots in Fig. 3), the spectra were fitted with reference data of metallic iron and Fe(II); note that the quantification may not be absolutely accurate, since the sputter process may create mixtures of different iron oxidation states. However, this quantitative evaluation indicates that the experiments with the 3 keV/1µA and 1 keV/1 µA parameter sets show a very similar tendency: only for the first few sputter levels does the higher acceleration voltage show a greater impact on the degradation kinetics. The experiment with 1 keV and 0.5 µA exhibited slower conversion to elemental Fe. In order to obtain a rough estimate of when approximately 20 at.% of metallic Fe species were formed, the etch times were read from the plots: 3000 s (3 keV, 1 µA), 3500 s (1 keV, 1 µA) and 6000 s (1 keV, 0.5 µA), as seen in Fig. 3. Once more, the ion ranges of Ar^+ ions in Fe(II) oxide and in Fe(III) oxide were simulated, and the sputter rates were roughly estimated using TRIM simulations [16]. FeO sputtered with 3 keV and 1µA exhibited an ion penetration depth of 26 Å and a sputter rate of ~7.46 nm/min; for 1 keV and 1 µA Ar^+ ions, the ion range was 14 Å and the estimated sputter rate ~4.49 nm/min, and for1 keV and 0.5 µA it was ~2.24 nm/min. The simulation of Fe_2O_3 yielded similar results: ion ranges of 27 Å, 15 Å and 15Å and etch rates of 7.57 nm/min, 4.54 nm/min and 2.27 nm/min were obtained for the 3 keV/1uA, 1keV/1uA and 1keV/0.5uA parameter sets, respectively. Again, the average

surface binding energies were deduced from the simulations of FeO and Fe_2O_3, which gave 3.2 eV in both cases. For all quantitative plots (see Fig. 3), an additional axis showing the ion etch depth calculated based on the simulated sputter yields is given. At a depth of 1 µm, nearly independently of the sputter parameters, one would find approximately 25 at.% of metallic Fe species formed by decomposition; using a lower ion current is not an effective means of avoiding sample alteration. A decreased current results in a proportionally decreased sputter rate; hence, in order to remove the same amount of material, the sample must be exposed longer to the ion bombardment, which in turn leads to a similar degradation. As shown in Fig. 3, for the first few etch levels the experiment using the kinetic energy of 3 keV results in a faster alteration compared to the one with 1 keV. Considering the axis that shows the individual sputter depths, the sputter damage appears to be slightly lower for the higher acceleration voltage, which may be related to a shorter exposure time to the ion beam. Based on these results, it is necessary to find an approach that avoids this high ratio of degraded to removed volume.

3.3. Ar cluster sputtering on $Zn_5(CO_3)_2(OH)_6$

Since both hydrozincite and iron(II) oxide (in this context also iron(III) oxide) showed severe chemical degradation by monoatomic argon ion sputtering despite using the "gentler" etch parameters, we decided to examine the potential of a different and more sophisticated etch technique, namely Ar cluster sputtering. The strength of this concept lies in the fact that the clusters dissociate upon contact with the sample surface; *i.e.*, the cluster energy is distributed to the total number of cluster atoms. As these atoms have a low penetration depth, causing shallow sputter craters, we expected shallower sputter damage and the sputter artefact of atomic mixing to be less strongly developed. Due to the low penetration depth, the number of implanted Ar atoms remaining in the sample material is relatively low [27]. Another advantage is the very low charge per cluster atom, since the total cluster charge (which equals at most a few elemental charges) is divided by the number of cluster atoms [28]. In our experiment, the hydrozincite powder was applied to a piece of adhesive carbon tape and exposed to a long-term sputter experiment with a cluster size of 2000 atoms and a kinetic energy of 4 keV. The initial sputter duration was 400 s performed 5 times, followed by 10 steps of 1200 s each and 5 steps of 2400 s each. The resulting spectra and quantitative data of the evolution of the O1s signals over the etch time are presented in Fig. 4.

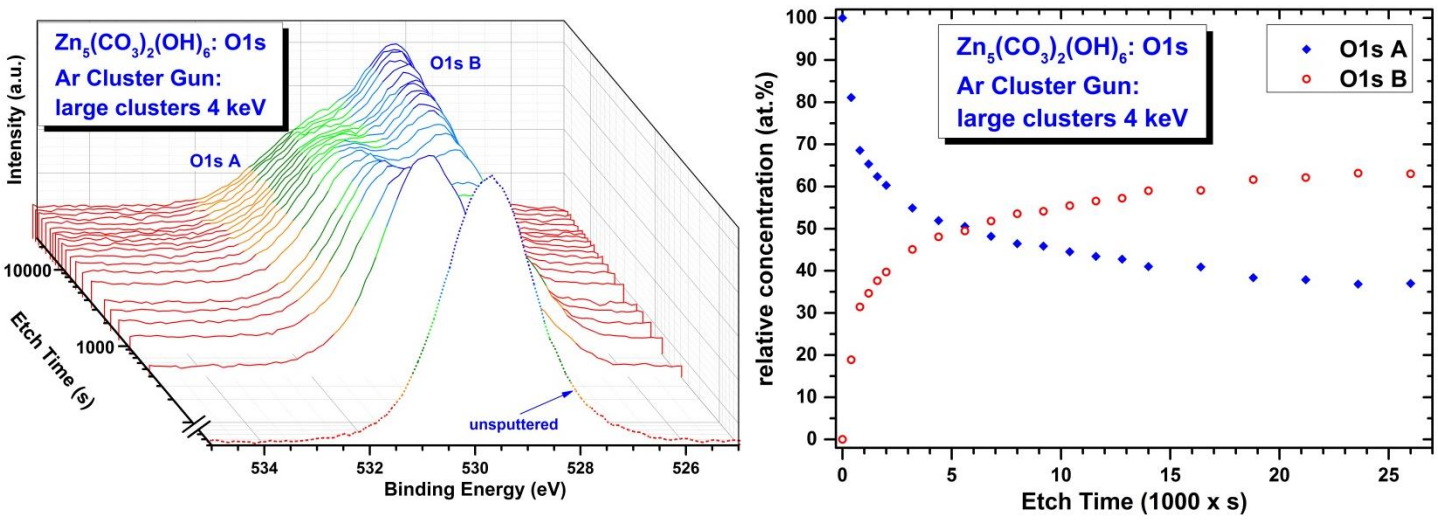

Fig. 4 Evolution of the O1s spectra of hydrozincite as functions of sputter time, acquired during long-term Ar cluster sputtering using a large cluster size and a cluster energy of 4 keV is shown. The deduced decomposition kinetics of O1s A to O1s B over etch time are additionally presented.

It can be seen that sputtering with large argon clusters of moderate kinetic energy is not sufficient to fully hinder chemical modification of the sample. Again, the formation of a ZnO like species or a mainly ZnO containing compound is likely, which is supported by the calculated average MAP with 2009.62 ± 0.19 eV, and with a steadily increasing MAP as a function of sputter time. The elemental composition showed an increase in the Zn signal, while the oxygen and carbonate signals decreased. The quantitative evolution of the O1s A and O1s B signals, as shown in Fig. 4, clearly revealed decomposition kinetics that are much slower than for all three monoatomic etch experiments, including that with the cooled sample. Initially, this may be considered a partial success, but an important element of uncertainty is the unknown sputter rate: it is not known how much of the surface was removed compared to the damage causing bombardment. In the worst case, the surface is not removed and merely chemically altered. In this case, no fresh or less affected material from underneath contributes to the XPS information volume. The degradation triggered by the monoatomic ions, each carrying energy in the range of some keV, is expected to be stronger than that caused by the atoms dissociated from the clusters, since in our experiment their energy would amount to only ~2 eV/atom. However, even this low energy may be sufficient to disrupt bonds of hydrozincite. In order to remove a surface atom, the surface binding energy must be exceeded by energy transfer from the collision cascade. As this surface binding energy is only documented for a small number of materials, a good approach to estimating this sputter threshold value is to use the heat of sublimation [29,30] or multiples of this parameter [31]. In this context, the obtained average surface binding energy of hydrozincite of 3.6 eV and the energy carried by each cluster atom with

~2 eV/atom seem to prevent any sputter removal. Nevertheless, according to Matsuo *et al.* [28] for large clusters the sputter threshold energy is significantly lower than for monoatomic ions because cluster sputtering involves the collision of a very high number of particles in a small volume, and interactions with other, neighbouring collision cascades must also be considered.

3.4. Ar cluster sputtering on FeO

The performance of Ar cluster sputtering was tested not only on hydrozincite but also on Fe(II) oxide to determine its potential for surface cleaning and recording XPS depth profiles. In general, spectra acquired on different XPS setups should be consistent, but since iron oxides do not exhibit trivial symmetric Gaussian-Lorentzian-shaped peaks (asymmetric peaks occur due to multiplet splitting and shake-up structures) and the XPS systems used were equipped with different charge build-up neutralisation techniques, which may have an impact on parameters such as the FWHM, spectra of the original sample surface were taken by both systems and compared in an overlay (see Fig. 5).

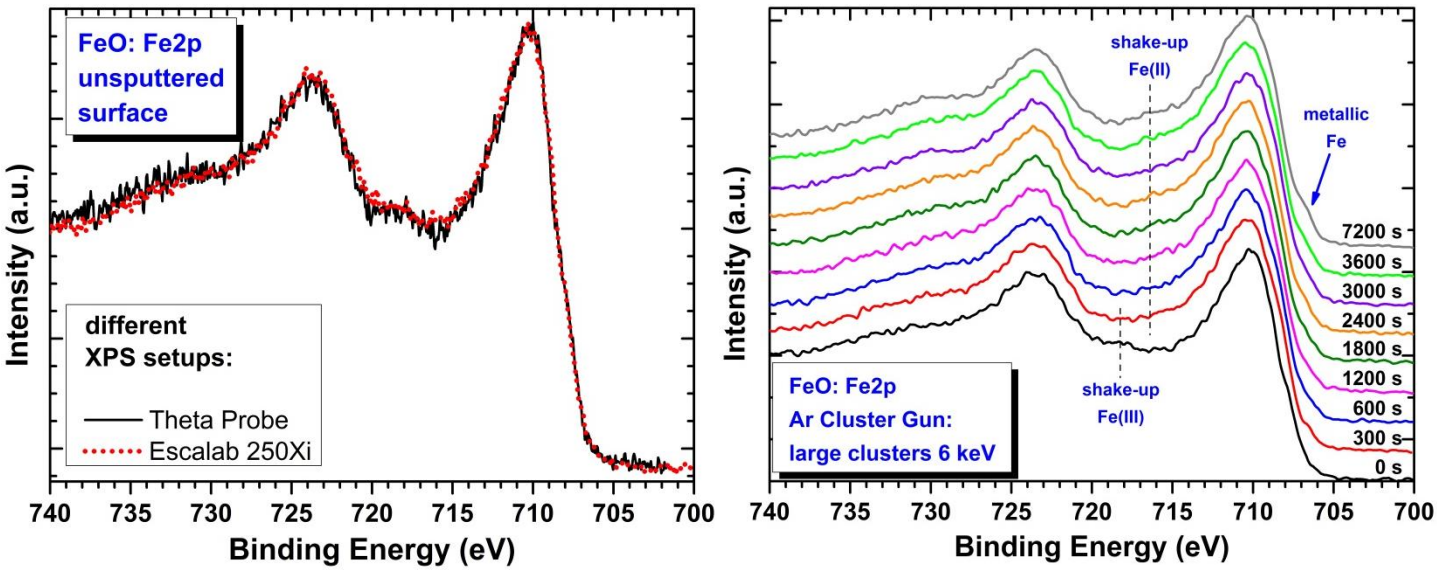

Fig. 5 Left: Overlay of the Fe2p spectra of the unsputtered surface of iron(II) oxide, acquired with a Theta Probe XPS system and an Escalab 250Xi. Right: Evolution of the Fe2p spectra of FeO as functions of sputter time, acquired during long-term Ar cluster sputtering using a large cluster size and cluster energy of 6 keV.

It is obvious that both spectra shown in the left-hand plot (after alignment and normalisation of the intensity signals) are equivalent, *i.e.*, show the same peak features with identical peak ratios and binding

energies. Thus, no concerns about the comparability of iron oxide data obtained from the Theta Probe and Escalab 250Xi setups should remain.

In our first Ar cluster sputter experiment, we used a large cluster size (2000 atoms) and a cluster energy of 6 keV; the sputter duration was 300 s performed 2 times, then 5 steps of sputtering for 600 s, followed by 1 period of 3600 s (as shown in the right part of Fig. 5). It can be seen that Ar cluster etching using a cluster energy of 6 keV already removed the Fe(III) species, which was originally present on top of the Fe(II), after one sputter step lasting 300 s, as indicated by the position of the corresponding shake-up satellites in the spectra. After some further sputter cycles, the formation of a shoulder at lower binding energy after 7200 s is visible, which hints at metallic iron; *i.e.*, the sample was again chemically altered. In order to test whether the lower voltage of 4 keV in combination with large clusters is more appropriate for profiling, and to verify whether a chemically transformed sample can be "repaired" by gentle sputtering, a deliberately damaged surface was prepared using the monoatomic mode of the cluster gun with an energy of 3 keV per Ar^+ ion. Subsequently, 2 argon cluster etch steps followed, each lasting 600 s. The resulting spectra are shown in the left plot in Fig. 6; additionally, a spectrum of an unsputtered FeO surface, consisting of naturally formed Fe(III) oxide, is given.

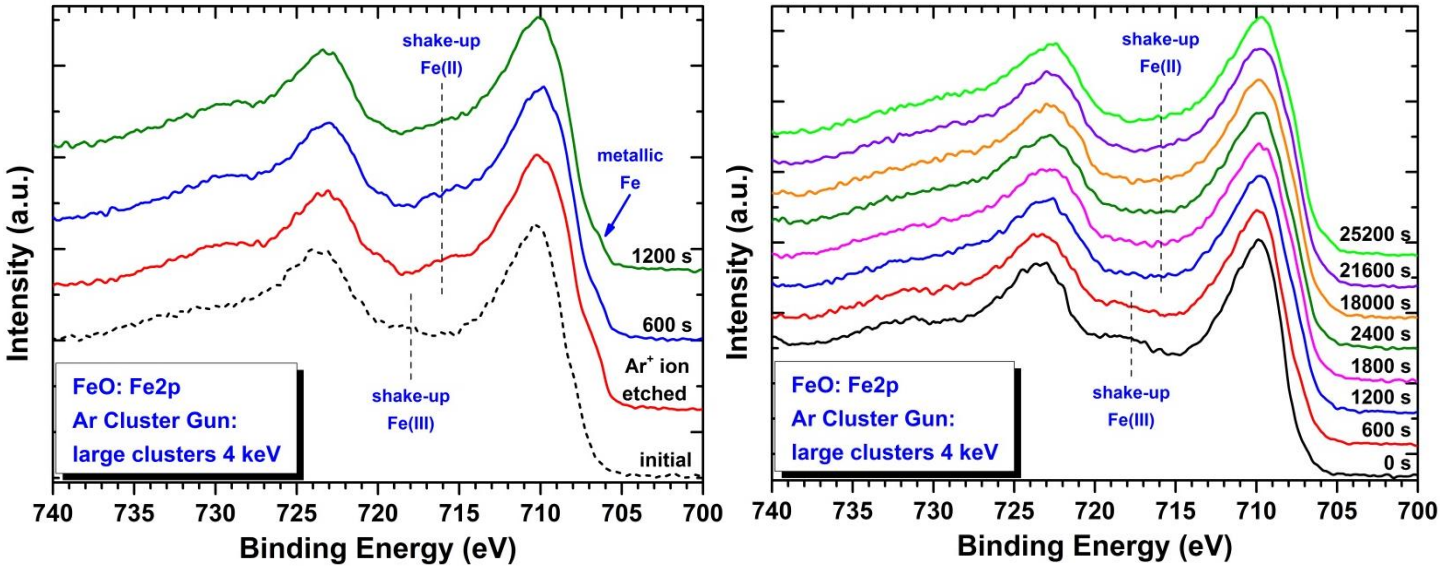

Fig. 6 Left: Fe2p spectra of FeO, which was initially intentionally degraded by Ar^+ ion bombardment, and subsequently sputtered with Ar clusters using a large cluster size and cluster energy of 4 keV. Right: Evolution of the Fe2p spectra of a fresh FeO sample as functions of sputter time, acquired during long-term Ar cluster sputtering using a large cluster size and cluster energy of 4 keV.

It can be seen that the damaged surface, which showed indications of iron in the metallic state, is slowly changed by gentle erosion to a "correct" composition that consists solely of material in the Fe(II) oxidation state. This decrease in the metallic Fe content indicates that a cluster energy of 4 keV might be sufficiently high to remove atoms from the surface by sputtering. In addition, this set of parameters (4 keV and a large cluster size) was applied using a fresh sample of FeO (see the right-hand plot in Fig. 6). After sputtering for 1200 s, the shake-up satellite as an indicator for Fe(III) vanished, and that of Fe(II) became visible. Even after long-term sputtering (up to 7 h), no evidence of a further reduction in the Fe(II) state to the lower state of elemental iron was observable. The sample seems to remain stable using these etch conditions. Next, this sputter etched sample was used to examine the influence of 2 keV sputtering with a large cluster size: the experiment was continued at the same position with 9 sputter steps of 1800 s each. Fig. 7 presents the resulting evolution of the Fe2p spectra (for better visibility some etch levels were left out).

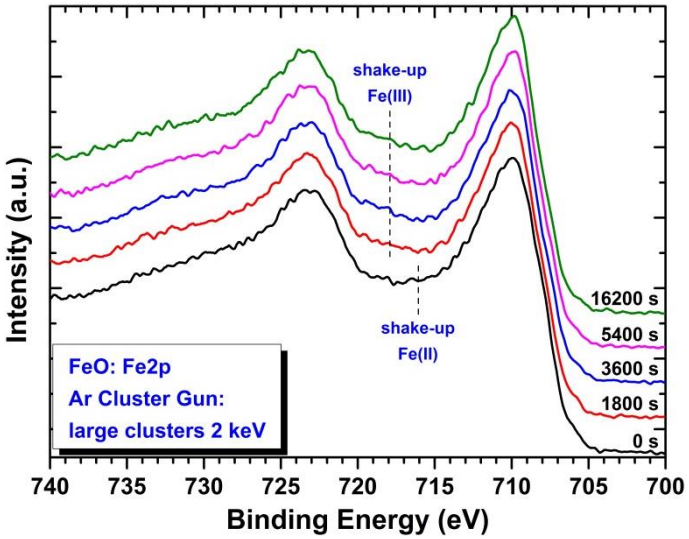

Fig. 7 Evolution of the Fe2p spectra of iron(II) oxide as functions of sputter time, acquired during long-term Ar cluster sputtering using a large cluster size and cluster energy of 2 keV.

Interestingly, after etching for 1800 s, a shifting of the shake-up feature of the $Fe2p_{3/2}$ signal is observable. This new position is indicative of the transformation of the initial Fe(II) to Fe(III) oxidation state. The following levels do not show any further changes, even for long-term etching. In order to identify the reason for the observed oxidation, we used the Theta Probe system and a new FeO sample that was intentionally damaged by short-term Ar^+ ion etching until only the Fe(II) state was visible. The sample was kept in position without any further exposition to ion bombardment or X-ray irradiation. High resolution spectra of the Fe2p and O1s levels taken after more than 24 h revealed no significant change, *i.e.*, no potential oxidation to an Fe(III) species by the oxygen content in the residual gas of the UHV

chamber. To find out whether a driving force is needed to initiate oxidation, the sample was subsequently irradiated for 6 h by X-rays and the dual flood gun, but again no conversion to an Fe(III) species could be observed. The exact reason for the observed change in the oxidation state due to cluster bombardment with 2 keV could not be found; we assume that this effect is related to surface modifications without material removal and/or the influence of the residual gas, which could not be confirmed on the Theta Probe setup, since the damaged volume is expected to be substantially different. Further, the average surface binding energy for Fe(II) oxide and for Fe(III) oxide (approximately 3.2 eV) neither confirms nor excludes that the surface atoms are sputter removed by clusters dissociating into atoms with 1 eV or 2 eV kinetic energy, since cluster sputtering does not follow the same rules as monoatomic ion sputtering.

3.5. He^+ ion sputtering on $Zn_5(CO_3)_2(OH)_6$

In general, the sputter yield and consequently the sputter rate depend on various factors, for instance, angle of incidence, ion energy, crystal orientation (in the case of crystalline samples), masses and surface binding energy of the target atoms and also of the mass of the projectile ions [32]. In order to find an approach suited to surface cleaning if not to depth profiling (due to the excessively low sputter rate), we tested an extreme ion type. We selected erosion with He^+ ions, which carry a much lower momentum according to the relationship between kinetic energy, mass and momentum. For this experiment, the O1s spectra of hydrozincite are presented once more as functions of sputter time (see Fig. 8).

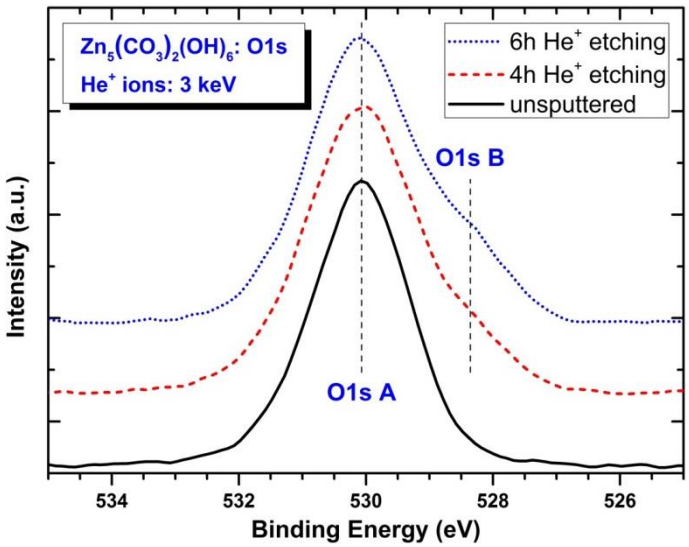

Fig. 8 Evolution of the O1s spectra of hydrozincite sputtered with He^+ ions using an acceleration voltage of 3 keV.

As can be seen in the lower binding energy region of the figure, a shoulder forms next to the original oxygen peak with an increase in etch time. Fits of these spectra yielded approximated O1s A/O1s B ratios of 84 to 16 at.% and 80 to 20 at.% after 4 h and 6 h of He^+ sputtering, respectively. In addition, the elemental composition deviated from the expected stoichiometry; again, an increasing Zn signal was observed, and the carbonate concentration decreased steadily (from its initial value, the carbonate signal dropped respectively to ~8.2 at.% and ~7.5 at.% after 4 h and 6 h of sputtering). Based on these results, no sputter method that is non-destructive to this kind of potential corrosion product could be found. Compared to the other approaches investigated, He^+ sputtering exhibited the smallest negative impact. Sputter removal is expected to be minimal, as indicated by TRIM simulations [16], which resulted in a sputter yield of 0.21 atoms/ion for Zn, 0.34 atoms/ion for O and 0.02 atoms/ion for carbon and an ion range of 217 Å. Furthermore, this assumption is supported by the observation that the low amount (only a few at.%) of adventitious carbon contamination initially present on the surface could not be totally eliminated.

Nearly none of the approaches tested was effective for the chosen materials for sputter depth profiling or for surface cleaning without noticeable change in the chemical composition or excessive cost in experimental time; only cluster sputtering using 4 keV seems to have potential for practical use. Sample degradation or alteration caused by the measurement method itself is, however, the crucial issue in XPS investigations, since the potential to resolve different chemical species cannot be used without restriction in case of materials that are sensitive to X-rays, dual flood gun exposure or ion/cluster bombardment [20,21,5]. Hence, it is absolutely necessary to keep these facts in mind, and – as far as possible – complementary methods must be employed to gain additional insights and evaluate the resulting XPS data. In addition, it is good practise to perform short stability tests to confirm that the material of interest remains stable throughout the investigation. Since sputter depth profiling in combination with photoelectron spectroscopy is a commonly used concept, *e.g.* [1,2,3], we again note that the results obtained (especially quantification) may be less accurate than they appear. When we consider the following three important corrosion products of Zn and Zn-alloy coated steel - hydrozincite, simonkolleite and zinc hydroxide - ion etching may at first lead to the erroneous assumption of the appearance or enrichment of zinc oxide at depth. In relation to developments in sputter equipment, it is notable that, in addition to Ar cluster guns [9], sources of buckminsterfullerene clusters [33] have been available for some time. We anticipate that oxygen cluster guns will soon be used in common commercial setups, where they may provide higher sputter rates than argon clusters for inorganic compounds. In order to find a suitable method for the challenging field of depth profiling, the potential of these methods should be discussed and tested.

4. Conclusions

Changes of the chemical states of hydrozincite and iron(II) oxide, two potential corrosion products of Zn-coated steel, were investigated for different sputter techniques and parameters. At first, these materials were tested for monoatomic Ar^+ ion etching by using modified sets of the sputter parameters, namely decreased acceleration voltage and ion current. Lower target temperature (*i.e.*, cooling) and a different type of projectile ions with lower mass were included in these investigations. Additionally, Ar cluster sputtering with various cluster energies was tested. In general, a chemical alteration of the materials could not be fully prevented; only the decomposition kinetics could be slowed down, but at the expense of the sputter rate. The promise of cluster sputtering may remain limited, since in most cases degradation persisted and the effective sputter removal rate remained undetermined; sputtering of Fe(II) oxide using medium cluster energy appears to be the only effective method. We therefore conclude that evaluation should use all of the experimental information collected and – if possible – consider complementary analytical techniques when acquiring depth profiles to identify different chemical states in case the stability of compounds potentially present is not guaranteed.

Acknowledgements

Financial support by the Austrian Federal Ministry of Science, Research and Economy and the National Foundation for Research, Technology and Development is gratefully acknowledged.

References

[1] E. Diler, S. Rioual, B. Lescop, D. Thierry, B. Rouvellou, Chemistry of corrosion products of Zn and MgZn pure phases under atmospheric conditions, Corros. Sci. 65 (2012) 178-186.

[2] E. Diler, B. Lescop, S. Rioual, G. Nguyen Vien, D. Thierry, B. Rouvellou, Initial formation of corrosion products on pure zinc and MgZn2 examinated by XPS, Corros. Sci. 79 (2014) 83-88.

[3] E. Diler, B. Rouvellou, S. Rioual, B. Lescop, G. Nguyen Vien, D. Thierry, Characterization of corrosion products of Zn and Zn–Mg–Al coated steel in a marine atmosphere, Corros. Sci. 87 (2014) 111-117.

[4] T. Prosek, A. Nazarov, U. Bexell, D. Thierry, J. Serak, Corrosion mechanism of model zinc-magnesium alloys in atmospheric conditions, Corros. Sci. 50 (2008) 2216–2231.

[5] R. Steinberger, J. Duchoslav, M. Arndt, D. Stifter, X-ray photoelectron spectroscopy of the effects of Ar^+ ion sputtering on the nature of some standard compounds of Zn, Cr, and Fe, Corros. Sci. 82 (2014) 154-164.

[6] E. Lewin, M. Gorgoi, F. Schäfers, S. Svensson, U. Jansson, Influence of sputter damage on the XPS analysis of metastable nanocomposite coatings, Surf. Coat. Tech. 204 (2009) 455-462.

[7] D.-J. Yun, J. Chung, C. Jung, K.H. Kim, W. Baek, H. Han, B. Anass, G.S. Park, S.H. Park, An electronic structure reinterpretation of the organic semiconductor/electrode interface based on argon gas cluster ion beam sputtering investigations, J. Appl. Phys. 114 (2013) 013703-1 - 013703-8.

[8] I. Yamada, A short review of ionized cluster beam technology, Nucl. Instrum. Meth. B 99 (1995) 240-243.

[9] P.J. Cumpson, J.F. Portoles, A.J. Barlow, N. Sano, Accurate argon cluster-ion sputter yields: Measured yields and effect of the sputter threshold in practical depth-profiling by x-ray photoelectron spectroscopy and secondary ion mass spectrometry, J. Appl. Phys. 114 (2013) 124313-1 - 124313-8.

[10] Y. Yamamoto, K. Yamamoto, Ar ion damage on the surface of soda-lime-silica glass, Mater. Sci. Eng. 18 (2011) doi: 10.1088/1757-899X/18/2/022005.

[11] L.S. Chang, Y.C. Lin, C.Y. Su, H.C. Wu, J.P. Pan, Effect of C60 ion sputtering on the compositional depth profiling in XPS for Li(Ni,Co,Mn)O2 electrodes, Appl. Surf. Sci. 258 (2011) 1279-1281.

[12] T. Miyayama, N. Sanada, M. Suzuki, J.S. Hammond, S.Q.D. Si, A. Takahara, X-ray photoelectron spectroscopy study of polyimide thin films with Ar cluster ion depth profiling, J. Vac. Sci. Technol. A 28 (2010) L1-L4.

[13] R. Grilli, R. Simpson, C.F. Mallinson, M.A. Baker, Comparison of Ar^+ Monoatomic and Cluster Ion Sputtering of Ta_2O_5 at Different Ion Energies, by XPS: Part 2 - Cluster Ions, Surf. Sci. Spectra 21 (2014) 68-83.

[14] C.D. Wagner, Auger lines in X-ray photoelectron spectrometry, Anal. Chem. 44 (1972) 967–973.

[15] C.D. Wagner, W.M. Riggs, L.E. Davis, J.F. Moulder, Handbook of X-ray Photoelectron Spectroscopy, first edition, Perkin-Elmer Corporation, Minnesota, 1979.

[16] J.F. Ziegler, J.P. Biersack, The Stopping and Range of Ions in Solids, SRIM-Software 2013 including TRIM calculation.

[17] G.K. Wehner, Sputtering by Ion Bombardment, Adv. Electron El. Phys. 7 (1955) 239-298.

[18] Z.L. Liau, B.Y. Tsaur, J.W. Mayer, Influence of atomic mixing and preferential sputtering on depth profiles and interfaces, J. Vac. Sci. Technol. 16 (1979) 121-127.

[19] V.I. Shulga, W. Eckstein, Depth of origin of sputtered atoms for elemental targets, Nucl. Instrum. Meth. B 145 (1998) 492-502.

[20] J. Duchoslav, R. Steinberger, M. Arndt, D. Stifter, XPS Study of Zinc Hydroxide as a Potential Corrosion Product of Zinc: Rapid X-ray Induced Conversion into Zinc Oxide, Corros. Sci. 82 (2014) 356-361.

[21] R. Steinberger, J. Duchoslav, T. Greunz, M. Arndt, D. Stifter, Investigation of the chemical stability of different Cr(VI) based compounds during regular X-ray photoelectron spectroscopy measurements, Corros. Sci. 90 (2015) 562-571.

[22] C.E. Carlston, G.D. Magnuson, A. Comeaux, P. Mahadevan, Effect of Elevated Temperatures on Sputtering Yields, Phys. Rev. 138 (1965) A759-A763.

[23] H. Shimizu, M. Ono, K. Nakayama, Effect of target temperature on surface composition changes of Cu-Ni alloys during Ar ion bombardment, J. Appl. Phys. 46 (1975) 460-462.

[24] S.R. Bhattacharyya, D. Ghose, D. Basu, Temperature dependence of sputtering yield of GaAs under 30 keV Ar^+ bombardment, J. Mater. Sci. Lett. 13(1994) 1192-1194.

[25] C.R. Brundle, T.J. Chuang, K. Wandelt, Core and valence level photoemission study of iron oxide surfaces and the oxidation of iron, Surf. Sci. 68 (1977) 459-468.

[26] T.J. Chuang, C.R. Brundle, K. Wandelt, An X-ray photoelectron spectroscopy study of the chemical changes in oxide and hydroxide surfaces induced by Ar+ ion bombardment, Thin Solid Films 53 (1978) 19-27.

[27] I. Yamada, W.L. Brown, J.A. Norhtby, M. Sosnowski, Surface modification with gas cluster ion beams, Nucl. Instrum. Meth. B 79 (1993) 223.

[28] J. Matsuo, N. Toyoda, M. Akizuki, I. Yamada, Sputtering of elemental metals by Ar cluster ions, Nucl. Instrum. Meth. B 121 (1997) 459-463.

[29] J.F. Ziegler, J.P. Biersack, Tutorial #2 - Target Mixing and Sputtering, SRIM-Software including TRIM calculation.

[30] R. Behrisch, W. Eckstein, Sputtering by Particle Bombardment: Experiments and Computer Calculations from Threshold to MeV Energies, Springer Berlin Heidelberg New York, 2007.

[31] M.A. Mantenieks, Sputtering Threshold Energies of Heavy Ions, 25th International Electric Propulsion Conference (1999).

[32] A.W. Czanderna, Methods of surface analysis, fifth impression, Elsevier Science Publishers B. V., The Netherlands, 1989.

[33] S. Sun, A. Wucher, C. Szakal, N. Winograd, Depth profiling of polycrystalline multilayers using a Buckminsterfullerene projectile, Appl. Phys. Lett. 84 (2004) 5177-5179.